Performance Analysis of Strained Monolayer MoS_2 MOSFET

Amretashis Sengupta, *Member, IEEE*, Ram Krishna Ghosh, and Santanu Mahapatra, *Senior Member, IEEE*

***Abstract*— We present a computational study on the impact of tensile/compressive uniaxial (ε_{xx}) and biaxial ($\varepsilon_{xx} = \varepsilon_{yy}$) strain on monolayer MoS_2, n-, and p-MOSFETs. The material properties like band structure, carrier effective mass, and the multiband Hamiltonian of the channel are evaluated using the density functional theory. Using these parameters, self-consistent Poisson–Schrödinger solution under the nonequilibrium Green's function formalism is carried out to simulate the MOS device characteristics. 1.75% uniaxial tensile strain is found to provide a minor (6%) ON current improvement for the n-MOSFET, whereas same amount of biaxial tensile strain is found to considerably improve the p-MOSFET ON currents by 2–3 times. Compressive strain, however, degrades both n-MOS and p-MOS devices performance. It is also observed that the improvement in p-MOSFET can be attained only when the channel material becomes indirect gap in nature. We further study the performance degradation in the quasi-ballistic long-channel regime using a projected current method.**

***Index Terms*— Density functional theory (DFT), MoS_2, MOSFET, nonequilibrium Green's function (NEGF), strain.**

I. Introduction

AMONG the various classes of alternate channel materials under research, the 2-D materials having nonzero bandgap in their sheet form like the transition metal dichalcogenides (MX_2:M = Mo, W; X = S, Se, and Te) seem very promising for MOSFET applications. This is due to their better electrostatic integrity, optical transparency, mechanical flexibility, and the geometrical compatibility with the standard planar CMOS technology. Among such MX_2 materials the performance of MoS_2-based MOS transistor and logic have been successfully demonstrated experimentally [1], [2]. This has generated great interest in studying such nongraphene 2-D crystals for future MOSFET channel application [3]–[5].

The main challenge in such 2-D MoS_2 FETs, so far has been to overcome the low carrier mobility of channel [1], [2]. For Si CMOS, strain engineering has long been used to enhance carrier mobility and improve drive currents and other device parameters [6]. Recent reports suggest that monolayer MoS_2 and other MX_2 also show alteration of material properties like band structure and carrier effective masses under the influence of strain [7]–[10]. In addition, Ghorbani-Asl *et. al.* in [11] have shown the impact of strain on the conductance in MoS_2 sheets. Hence, strain engineering in principle, could be used to improve the performance of MoS_2. In this paper, we investigate the impact of tensile and compressive uniaxial (ε_{xx}) and biaxial ($\varepsilon_{xx} = \varepsilon_{yy}$) strain on the performance of monolayer MoS_2, n-MOS, and p-MOS devices. In this paper, the material properties of 2-D (monolayer) MoS_2, like band structure, carrier effective mass, and the multiband Hamiltonian of the channel, were evaluated using the density functional theory (DFT). Using these parameters, the MOS device output characteristics were simulated by solving the Poisson and the Schrödinger equations self-consistently for the system, under the nonequilibrium Green's function (NEGF) formalism. The device simulation results show only a minor performance enhancement for the n-MOSFET under uniaxial tensile strain. On the other hand, the p-MOSFET performance is significantly improved by reducing the carrier effective mass by applying biaxial tensile strain.

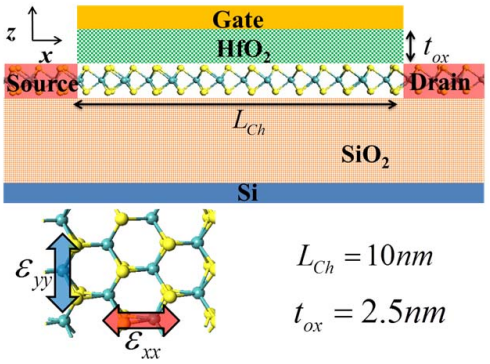

Fig. 1. Device schematic (not to scale) and diagram showing the applied uniaxial and biaxial tensile and compressive strains. We consider doped source and drains. $K \rightarrow \Gamma$ direction is taken as the transport direction.

II. Methodology

Fig. 1 shows the schematic device structure of the planar 2-D MoS_2 FET considered for our research. We consider a monolayer MoS_2 as the channel material, with channel length (L_{Ch}) of 10 nm. As shown in Fig. 1, the tensile and the compressive strains are considered applied in the two perpendicular directions x and y in the plane of the 2-D sheet. For uniaxial strain only ε_{xx} is applied whereas for

Manuscript received February 7, 2013; revised June 19, 2013; accepted July 12, 2013. Date of publication July 26, 2013; date of current version August 19, 2013. This work was supported in part by the Department of Science and Technology and Government of India under Grant SR/S3/EECE/0151/2012. The review of this paper was arranged by Editor A. Schenk.

The authors are with the NanoScale Device Research Laboratory, Department of Electronic Systems Engineering, Indian Institute of Science, Bangalore 560012, India (e-mail: amretashis@dese.iisc.ernet.in; ramki.phys@gmail.com; santanu@cedt.iisc.ernet.in).

Color versions of one or more of the figures in this paper are available online at http://ieeexplore.ieee.org.

Digital Object Identifier 10.1109/TED.2013.2273456

the biaxial case strain is applied in both x and y directions with $\varepsilon_{xx} = \varepsilon_{yy}$. The 2-D channel is placed over an SiO_2/Si substrate. High-κ HfO_2 of 2.5-nm thickness is chosen as the gate dielectric. We consider highly doped (10^{20} /cm^3) n^{++} and p^{++} regions as the source/drain for the n-MOSFET and the p-MOSFET, respectively. Such doping concentrations allow for a very good alignment of the source/drain Fermi levels with the conduction band/valence band for the monolayer MoS_2, n-, and p-MOSFETs [4], [5]. For our simulations, $K \rightarrow \Gamma$ direction (x direction in Fig. 1) is taken as the transport direction.

The first step, in this paper, is to evaluate the electronic properties of the channel material (i.e., strained and unstrained monolayer MoS_2 sheets). For this purpose, we employ DFT in QuantumWise Atomistix Tool Kit (ATK) [13]. We use a 16 × 16 × 1 Monkhorst-Pack k-grid [14], [15] and employ the localized density approximation [15] exchange correlation function with the double-zeta polarized (DZP) basis [14]. We use Troullier–Martins type norm-conserving pseudopotential sets in ATK (NC-FHI[z = 6] DZP for Sulfur and NC-FHI[z = 6] DZP for Molybdenum). Relativistic corrections are included in the nonlinear core [13]. Using DFT, we simulate the band structure and the electron and the hole effective masses of the monolayer MoS_2. The multiband 41 × 41 Hamiltonain matrix (H) and the nonorthogonal overlap matrix (S) are extracted from ATK at the valence band maxima (VB_{max}) and the conduction band minima (CB_{min}) of the band structure, for various strained and relaxed conditions. As with applied strain, the nature of the bandgap of the monolayer changes from direct to indirect gap, we extract the Hamiltonians at the corresponding CB_{min} for the n-MOSFET, and at the corresponding VB_{max} for the p-MOSFET simulations.

Thereafter, we proceed to solve the Poisson and Schrödinger equations self-consistently for our MoS_2 FET. The self-consistent solutions are carried out under the NEGF formalism [16], [17]. In our solver, we construct the Green's function from the knowledge of the H and S matrices and the energy eigenvalue matrix E of the system along with the self-energy matrices Σ_S and Σ_D of the source and drain contacts, respectively. The Green's function is then evaluated as [16] follows:

$$G(E) = [ES - H - \Sigma_S - \Sigma_D]^{-1}. \tag{1}$$

From (1), parameters like the broadening matrices $\wp_S$ and $\wp_D$ and the spectral densities A_S and A_D are evaluated using the following relations:

$$\wp_{S,D} = i[\Sigma_{S,D} - \Sigma^{+}_{S,D}]. \tag{2}$$

$$A_{S,D} = G\wp_{S,D}G^{+}. \tag{3}$$

The density matrix [$\Re$] used to solve the Poisson equation is given by

$$[\Re] = \int_{-\infty}^{\infty} \frac{dE}{2\pi}[A(E_{k,x})]f_0(E_{k,x} - \eta) \tag{4}$$

where $A(E_{k,x})$ is the spectral density matrix, $E_{k,x}$ is the energy of the conducting level, and η being the chemical potential

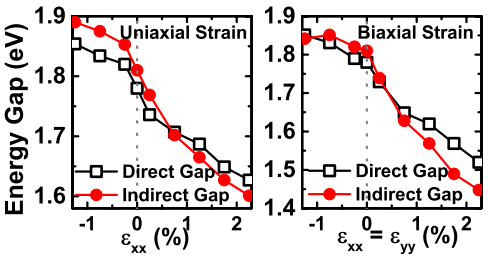

Fig. 2. Effect of uniaxial (ε_{xx}) and biaxial ($\varepsilon_{xx} = \varepsilon_{yy}$) tensile (+) and compressive (−) strain on the bandgap of the monolayer MoS_2.

of the contacts. $f_0(.)$ is the Fermi function. The transmission matrix $\Im(E)$ is calculated as follows:

$$\Im(E) = \text{trace}[A_S\wp_D] = \text{trace}[A_D\wp_S]. \tag{5}$$

Thus, giving out the ballistic drain current $I_{D,Bal}$ as [3] follows:

$$I_{D,Bal} = \frac{q}{\hbar^2}\sqrt{\frac{m_t\varphi_{Th}}{2\pi^3}}\int_{-\infty}^{\infty}\left[F_{-1/2}\left(\frac{\eta_S - E_{k,x}}{\varphi_{Th}}\right) - F_{-1/2}\left(\frac{\eta_D - E_{k,x}}{\varphi_{Th}}\right)\right]\Im(E_{k,x})dE \tag{6}$$

m_t being the carrier effective mass in the transverse direction, φ_{Th} is the thermal energy, $E_{k,x}$ is the energy of the conducting level, $F_{-1/2}$ is the Fermi integral of order $-1/2$. η_S and η_D are the chemical potentials of the source and drain, respectively. It is notable that the current calculated in (6) is purely ballistic in nature, which holds well for channels of short dimensions up to few tens of nanometers. However, for longer channel lengths the transmission encounters scattering, and becomes quasi-ballistic in nature. For considering these effects, we use a projection factor Θ to evaluate our MOSFET drain current as [3], [4] follows:

$$I_D = \Theta \times I_{D,Bal}. \tag{7}$$

The value of Θ is determined as follows:

$$\Theta = \frac{\lambda_{max}}{L_{Ch} + \lambda_{max}} \tag{8}$$

where L_{Ch} is the channel length and λ_{max} is the mean free path calculated as [3], [4] follows:

$$\lambda_{max} = \frac{(2\varphi_{Th})^{3/2}}{q\mu}\frac{F_0(\eta_S - E_C)}{F_{-1/2}(\eta_S - E_C)} \tag{9}$$

where E_C is the top of the conduction band energy in the channel, which is evaluated from the maxima of the self-consistent potential Φ_{SC} in the channel, $F_{-1/2}$ is the 1-D Fermi integral of order $-1/2$, and μ is the carrier mobility. It is worth noting that for short channel lengths, $\lambda_{max} \gg L_{Ch}$, and therefore $\Theta \rightarrow 1$, which is the purely ballistic case.

III. Results and Discussions

A. Materials Study With DFT

In Fig. 2, we have shown the impact of various uniaxial and biaxial tensile and compressive strains on the bandgap of the monolayer MoS_2. In the relaxed case, the band structure

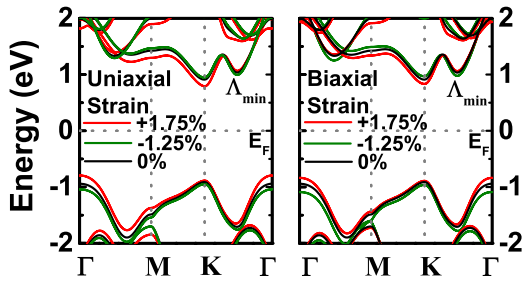

Fig. 3. Band structure of the MoS_2 sheet under different strain conditions.

is direct in nature, with the VB_{max} and CB_{min} both at the K point of the Brillouin zone (BZ). However, as we apply strain to the system the band structure changes and the MoS_2 undergoes transition from direct to an indirect gap material. It is seen that for uniaxial strain the material becomes indirect gap at tensile strain of $+1.25\%$ whereas for biaxial strain it becomes indirect for strains above $+0.75\%$. For uniaxial compressive strain, the band structure remains direct at the K point for strains up to -1.25% but for biaxial compressive strain of -1.25%, the material becomes indirect gap in nature. We have not shown compressive strains further than -1.25% as this increases the carrier effective mass (not shown here) and therefore is degenerative to device performance, as we shall see in the following section.

The direct bandgap is always measured at the K point of the BZ, for relaxed MoS_2 sheet it was found to be 1.78 eV, which is consistent with other DFT results [10]. In the relaxed condition, the monolayer MoS_2 shows a slightly higher indirect gap of 1.82 eV between the CB_{min} at K point and the VB_{max} at Γ point. In the different strained condition the indirect gap, however, is measured between the different sets of VB_{max} and CB_{min} as the band structure changes. In Fig. 3, we see that for tensile uniaxial and biaxial strain, the VB_{max} is at the Γ point while the CB_{min} remains at the K point. However, for the uniaxial and the biaxial compressive strain, the VB_{max} remains fixed at the K point but the CB_{min} tends to shift to a point in between the K point and the Γ point (i.e., in the Λ direction of the hexagonal BZ), which we shall designate as Λ_{min} hereafter. These band structure results are in good agreement with DFT results published by other groups [9], [10], [12].

Fig. 4 shows the variation of the carrier effective masses with applied strain at the different symmetry points (Γ, K, and Λ_{min}) of the BZ in different crystallographic directions. The $K \rightarrow \Gamma$ direction is referred to as the Λ direction, the $K \rightarrow M$ direction as T, and $\Gamma \rightarrow M$ direction as Σ. Thus, the legend $K(\Lambda)$ in Fig. 4, represents the carrier effective mass at the K point of the BZ in the $K \rightarrow \Gamma$ direction and $\Lambda_{min}(\Lambda)$ represents the carrier effective mass at the Λ_{min} point in the same direction, and so on. We can see that with the application of tensile strain, there is a slight reduction in the $K(\Lambda)$ and the $K(T)$ electron effective masses for both uniaxial and biaxial conditions. However, with uniaxial compressive strain, the electron effective masses increase. For biaxial compressive strain there is an increment in $K(\Lambda)$ and the $K(T)$ electron

TABLE I
ELECTRONIC BAND PROPERTIES UNDER UNIAXIAL STRAIN

$\varepsilon(\%)$	$\mathbf{VB}_{max}$	$\mathbf{CB}_{min}$	m_e	$m_{e,t}$	m_h	$m_{h,t}$
-1.25	K	K	$K(\Lambda)$	$K(T)$	$K(\Lambda)$	$K(T)$
-0.75	K	K	$K(\Lambda)$	$K(T)$	$K(\Lambda)$	$K(T)$
-0.25	K	K	$K(\Lambda)$	$K(T)$	$K(\Lambda)$	$K(T)$
0	K	K	$K(\Lambda)$	$K(T)$	$K(\Lambda)$	$K(T)$
+0.25	K	K	$K(\Lambda)$	$K(T)$	$K(\Lambda)$	$K(T)$
+0.75	Γ	K	$K(\Lambda)$	$K(T)$	$\Gamma(\Lambda)$	$\Gamma(\Sigma)$
+1.25	Γ	K	$K(\Lambda)$	$K(T)$	$\Gamma(\Lambda)$	$\Gamma(\Sigma)$
+1.75	Γ	K	$K(\Lambda)$	$K(T)$	$\Gamma(\Lambda)$	$\Gamma(\Sigma)$
+2.25	Γ	K	$K(\Lambda)$	$K(T)$	$\Gamma(\Lambda)$	$\Gamma(\Sigma)$

TABLE II
ELECTRONIC BAND PROPERTIES UNDER BIAXIAL STRAIN

$\varepsilon(\%)$	$\mathbf{VB}_{max}$	$\mathbf{CB}_{min}$	m_e	$m_{e,t}$	m_h	$m_{h,t}$
-1.25	K	Λ_{min}	$\Lambda_{min}(\Lambda)$	$\Lambda_{min}(T)$	$K(\Lambda)$	$K(T)$
-0.75	K	K	$K(\Lambda)$	$K(T)$	$K(\Lambda)$	$K(T)$
-0.25	K	K	$K(\Lambda)$	$K(T)$	$K(\Lambda)$	$K(T)$
0	K	K	$K(\Lambda)$	$K(T)$	$K(\Lambda)$	$K(T)$
+0.25	K	K	$K(\Lambda)$	$K(T)$	$K(\Lambda)$	$K(T)$
+0.75	Γ	K	$K(\Lambda)$	$K(T)$	$\Gamma(\Lambda)$	$\Gamma(\Sigma)$
+1.25	Γ	K	$K(\Lambda)$	$K(T)$	$\Gamma(\Lambda)$	$\Gamma(\Sigma)$
+1.75	Γ	K	$K(\Lambda)$	$K(T)$	$\Gamma(\Lambda)$	$\Gamma(\Sigma)$
+2.25	Γ	K	$K(\Lambda)$	$K(T)$	$\Gamma(\Lambda)$	$\Gamma(\Sigma)$

effective masses but a decrease in the $\Lambda_{min}(\Lambda)$ and $\Lambda_{min}(T)$ electron masses. As for the hole effective masses, there is not much change in the $K(\Lambda)$ and the $K(T)$ hole masses for uniaxial or biaxial tensile and compressive strain. However, for the hole effective mass in the $\Gamma(\Lambda)$ and the $\Gamma(\Sigma)$, there exists a significant change for biaxial strain. The values of electron and hole masses in the relaxed MoS_2 for $K(\Lambda)$ are 0.4750 m_0 and 0.5978 m_0, respectively. For $K(T)$, these values are 0.4741 m_0 and 0.5968 m_0, respectively. These results are consistent with other ab inito studies [7], [9], [10]. With the application of $+2.25\%$ biaxial strain, the hole effective mass could be brought down by 41% from its relaxed value. While for the electron a $+2.25\%$ uniaxial strain reduces the effective mass only by 3%. These values and the nature of the variation of electron and hole effective masses with uniaxial and biaxial strain on are consistent with the ab initio results published by others [10].

B. Device Simulation

Tables I and II show the location of the different VB_{max} and CB_{min} under varying uniaxial and biaxial strain along with the corresponding carrier masses that need to be considered for device simulation. Here, m_e and $m_{e,t}$ represent the electron masses in the transport and the transverse directions, respectively, whereas m_h and $m_{h,t}$ represent the hole masses for the same directions. The H and S matrices are extracted at those particular VB_{max} and CB_{min}, for p-MOS and n-MOS simulations, respectively.

Since for the performance enhancement of MoS_2 FET devices, the lowering of the carrier effective mass is essential [5]; hence for the simulations, we focus on the strains that decrease the carrier effective masses in our MOSFET devices. For the n-MOSFET, we consider

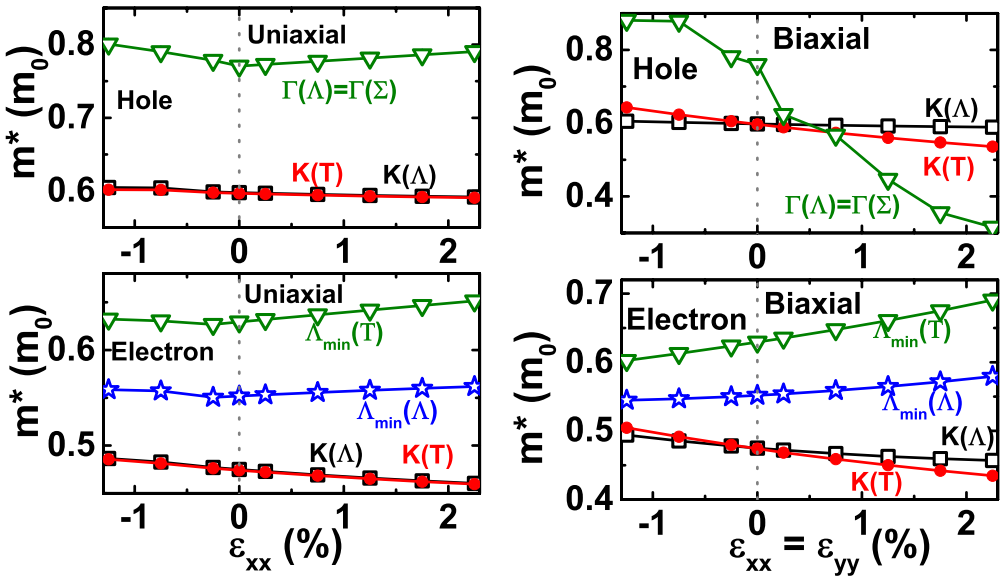

(a) (b)

Fig. 4. Electron and the hole effective masses in the monolayer MoS_2 channel for (a) uniaxial and (b) biaxial strain.

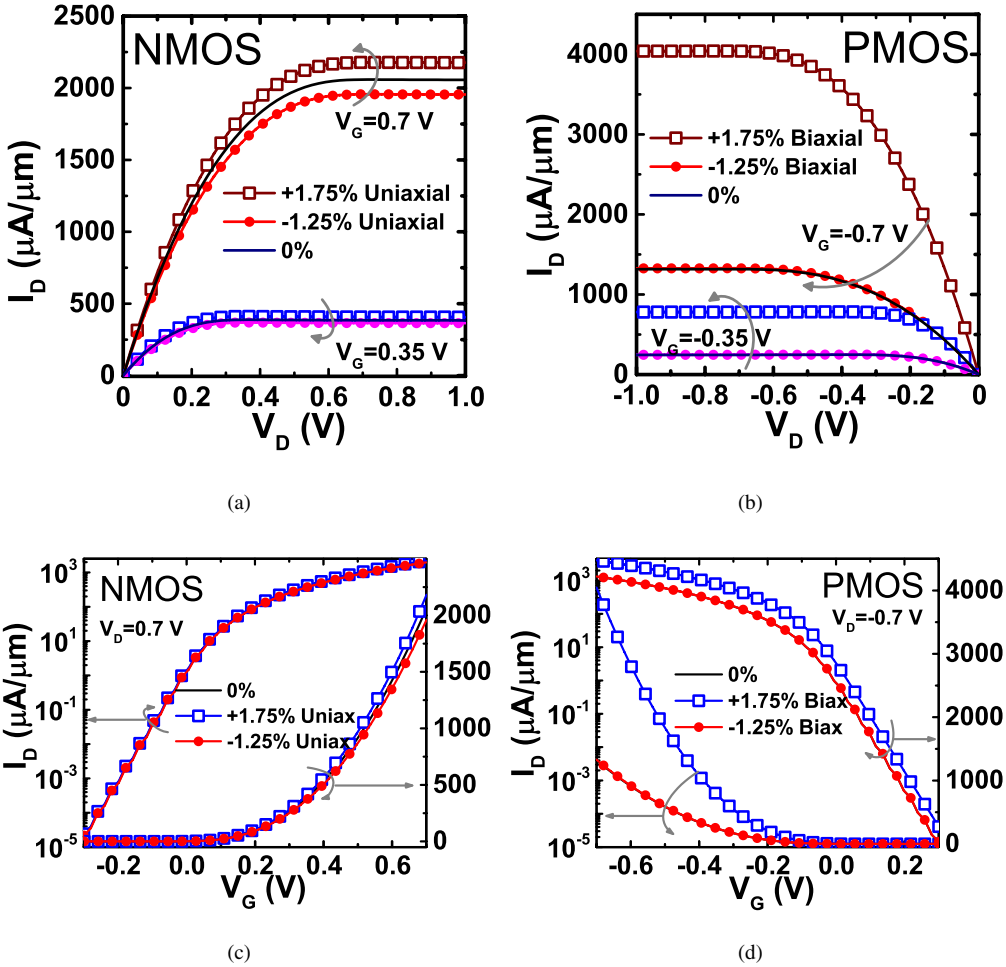

(a) (b)

(c) (d)

Fig. 5. (a) and (b) I_D–V_D and the (c) and (d) I_D–V_G characteristics of the n-MOS and p-MOS devices, with varying strain conditions.

the carrier masses under the uniaxial strain condition and for the p-MOSFET, we consider the biaxial strained condition.

The static dielectric constant $Re[\epsilon(\omega = 0)]$ of MoS_2 is evaluated from the optical spectra in ATK to be 3.92. This value is not affected by the applied strain (not shown).

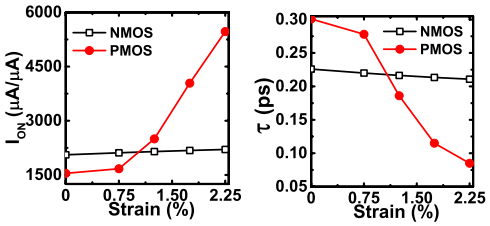

Fig. 6. Impact of strain on the (a) ON current and (b) intrinsic delay time of the MoS_2, n-, and p-MOSFETs. Uniaxial strain is considered for n-MOSFET and biaxial strain for p-MOSFET.

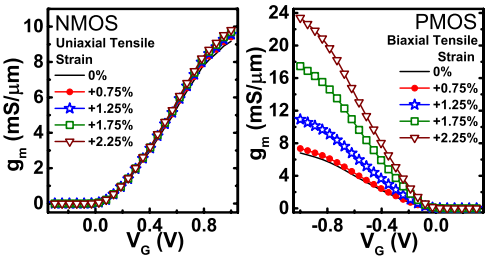

Fig. 7. Impact of strain on the transconductance (g_m) versus V_G plot of the MoS_2, n-, and p-MOSFETs.

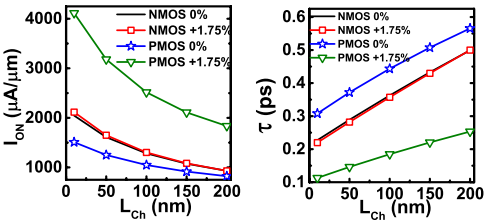

Fig. 8. Impact of channel length scaling on (a) ON current and (b) intrinsic delay time (τ) of the MoS_2, n-, and p-MOSFETs.

The I_D–V_D output characteristics (Fig. 5) of the n-MOSFET and p-MOSFET devices show the variation of drain current for varying applied strain and gate voltages. For comparison of the tensile and the compressive strains, we have shown the devices under three conditions, which are relaxed (0% strain), +1.75% strained, and −1.25% strained channels. As mentioned earlier, the nature of applied strain is uniaxial for the n-MOSFET and biaxial for the p-MOSFET, respectively.

The drive current value for the relaxed MoS_2 n-MOSFET is about 2058 μA/μm and that for the p-MOSFET is 1545 μA/μm, which is quite sufficient for the International Technology Roadmap for Semiconductors (ITRS) requirements for the 15 nm and lesser high-performance (HP) logic technology node [18]. We see that with application of +1.75% uniaxial strain the ON current for n-MOSFET could be increased to 2178 μA/μm, which is a 5.83% improvement over the relaxed value. However, for the −1.25% uniaxial strain, the n-MOS ON current decreases by about 4%. For the p-MOSFET, a very significant improvement is observed upon application of +1.75% biaxial strain. For this strain, the ON current becomes 4041 μA/μm, which is a two and a half fold increase over the relaxed ON current. In case of p-MOS, a slight degradation of ON current is observed for −1.25% biaxial strain. For +1.75% biaxial strain, the performance of the monolayer MoS_2 p-MOSFET can be greatly improved. In comparison with the p-MOSFET, the improvement in the n-MOSFET for an equal amount of uniaxial strain is just 6%. From our simulations, it is also observed that for both the n- and p-MOSFETs, applied strain does not impact the subthreshold slope (SS) significantly. Both strained and relaxed n- and p-MOSFETs show good immunity to short channel effects, with Drain Induced Barrier Lowering within the range 12–15 mV/V. The SS is calculated to be 60–62.5 mV/decade. The ON/OFF ratio is determined to be 10^8 considering V_{dd} = 0.7 V. These values are better than those for the Fully Depleted Silicon On Insulator and the MG MOSFET, for the 15-nm HP logic node, as recommended by ITRS [18].

The ON current and the intrinsic delay time improvement with applied tensile strain for the MoS_2 FETs are shown in Fig. 6. With increasing uniaxial tensile strain for the n-MOS device, and biaxial tensile strain for the p-MOS, significant improvement is observed in the ON currents and the delay time (τ) of these devices. For uniaxial strains of +2.25%, an increment of 7.2% can be brought about for n-MOS, whereas for the p-MOS, biaxial strain of the same magnitude can increase the ON currents by 3.6 times its relaxed value. For the same applied strain, the corresponding reduction in τ is about 18% for the n-MOSFET and almost 80% for the p-MOSFET.

In Fig. 7, we have shown the transconductance (g_m) versus gate voltage for the MOSFETs under consideration. For the simulation, V_D is set at 0.7 V. The value of g_m at the ON condition ($V_D = V_G = 0.7V$), for the n-MOSFET and the p-MOSFET in the relaxed condition are 7.2 and 7.5 mS/μm, respectively. For the strained condition, the g_m slightly increases up to 8 mS/μm for the n-MOSFET. For the p-MOSFET, the increment in g_m is much more prominent and in the ON condition, the value of g_m for +2.25% biaxially strained p-MOSFET reaches about 20.5 mS/μm.

So far, we have simulated all the results based on a 10-nm channel length (L_{Ch}) MOSFET. In such short channel length MoS_2 FET, the carrier transport is purely ballistic in nature and there is no scattering involved in the channel. For our simulations, we have considered such short L_{Ch} to analyze the performance of this new alternate channel material, in the HP technology node for next generation MOSFET application. However, most experimentally fabricated MoS_2 FET have L_{Ch} in the range of several hundred nanometers to few microns [1], [2]. In such long-channel devices, the carrier transport is no longer purely ballistic but quasi-ballistic in nature. To understand the performance of the strained MoS_2 FET in this region, we employ a projection method following Alam and Lake [4] and Yoon *et. al.* [3]. Using (7)–(9), we simulate the projected currents in the long-channel case. The ON current reduction and the increase in the intrinsic delay time for the n-MOS and the p-MOSFET in strained and relaxed conditions are shown in Fig. 8(a) and (b). As already discussed, we have considered uniaxial strain for the n-MOS and biaxial strain for the p-MOS device. For L_{Ch} = 200 nm, the reduction in

ON currents is 45% and 55% from the ballistic value, for the relaxed n- and the p-MOSFETs, respectively. However, for the strained p-MOS, this reduction is 55% that is slightly higher than relaxed value. For the strained n-MOS, however, the I_{ON} reduction remains the same. In fabricated long-channel devices, the reduction in drain current would be even higher owing to numerous defects and scattering centers formed during the processing. However, these projected currents give a good indication of the performance degradation for longer channel lengths.

As for the intrinsic delay time (τ) is concerned, it increases with an increasing L_{Ch} for all the devices. The delay time increases by around 1.8 times for the p-MOSFET and by 2.3 times for the n-MOSFET, as L_{Ch} is increased to 200 nm.

IV. Conclusion

The effect of varying tensile and compressive uniaxial and biaxial strain on the device performance of monolayer MoS_2, n-, and p-MOSFETs are studied herein. The material properties and the multiband Hamiltonian of the channel are evaluated using DFT. Using these parameters, the MOS device output have been simulated by self-consistent Poisson–Schrödinger equations solution, under NEGF formalism. Our researches show uniaxial tensile strain to be beneficial for n-MOSFET performance enhancement, whereas biaxial tensile strain shows to significantly improve the p-MOSFET performance. Compressive strain is found to be detrimental to the performance of both n- and p-MOSFETs. We also observe that the p-MOSFET performance enhancement is related to the transition of MoS_2 from direct to indirect bandgap material under applied strain. By a projection method performance, degradation of such strained MoS_2 FET in the quasi-ballistic region was also studied.

Acknowledgment

Dr. A. Sengupta would like to thank DST, Government of India, for the DST post-doctoral fellowship in nanoscience and technology. R.K. Ghosh would like to thank UGC-CSIR, Government of India, for his senior research fellowship.

References

[1] B. Radisavljevic, A. Radenovic, J. Brivio, V. Giacometti, and A. Kis, "Single-layer MoS_2 transistors," *Nature Nanotechnol.*, vol. 6, no. 3, pp. 147–150, Mar. 2011.

[2] B. Radisavljevic, M. B. Whitwick, and A. Kis, "Integrated circuits and logic operations based on single-layer MoS_2," *ACS Nano*, vol. 5, no. 12, pp. 9934–9938, Dec. 2011.

[3] Y. Yoon, K. Ganapathi, and S. Salahuddin, "How good can monolayer MoS_2 transistors be?" *Nano Lett.*, vol. 11, no. 9, pp. 3768–3773, Sep. 2011.

[4] K. Alam and R. K. Lake, "Monolayer MoS_2 transistors beyond the technology road map," *IEEE Trans. Electron Devices*, vol. 59, no. 12, pp. 3250–3254, Dec. 2012.

[5] L. Liu, S. B. Kumar, Y. Ouyang, and J. Guo, "Performance limits of monolayer transition metal dichalcogenide transistors," *IEEE Trans. Electron Devices*, vol. 58, no. 9, pp. 3042–3047, Sep. 2011.

[6] Y. Lee, K. Kakushima, K. Shiraishi, K. Natori, and H. Iwai, "Size-dependent properties of ballistic silicon nanowire field effect transistors," *J. Appl. Phys.*, vol. 107, no. 11, pp. 113705-1–113705-7, Jun. 2010.

[7] E. Scalise, M. Houssa, G. Pourtois, V. Afanasev, and A. Stesmans, "Strain-induced semiconductor to metal transition in the two-dimensional honeycomb structure of MoS_2," *Nano Res.*, vol. 5, no. 1, pp. 43–48, Jan. 2011.

[8] Q. Yue, J. Kang, Z. Shao, X. Zhang, S. Chang, G. Wang, S. Qin, and J. Li, "Mechanical and electronic properties of monolayer MoS_2 under elastic strain," *Phys. Lett. A*, vol. 376, nos. 12–13, pp. 1166–1170, Feb. 2012.

[9] P. Lu, X. Wu, W. Guo, and X. C. Zeng, "Strain-dependent electronic and magnetic properties of MoS_2 monolayer, bilayer, nanoribbons and nanotubes," *Phys. Chem. Chem. Phys.*, vol. 14, no. 37, pp. 13035–13040, Aug. 2012.

[10] H. Peelaers, and C. G. Van deWalle, "Effects of strain on band structure and effective masses in MoS_2," *Phys. Rev. B*, vol. 86, no. 24, p. 241401, Dec. 2012.

[11] M. Ghorbani-Asl, S. Borini, A. Kuc, and T. Heine, "Strain-dependent modulation of conductivity in single layer transition-metal dichalcogenides," *Phys. Rev. B*, vol. 87, no. 23, p. 235434, Jun. 2013.

[12] A. Kuc, N. Zibouche, and T. Heine, "Influence of quantum confinement on the electronic structure of the transition metal sulfide TS_2," *Phys. Rev. B*, vol. 83, no. 24, p. 245213, Jun. 2011.

[13] (2012). *QuantumWise Simulator, AtomistixToolKit(ATK)* [Online]. Available: http://www.quantumwise.com/

[14] H. J. Monkhorst and J. D. Pack, "Special points for Brillouin-zone integrations," *Phys. Rev. B*, vol. 13, no. 12, pp. 5188–5192, Jun. 1976.

[15] W. Kohn and L. J. Sham, "Self-consistent equations including exchange and correlation effects," *Phys. Rev.*, vol. 140, no. 4A, pp. A1133–A1138, Nov. 1965.

[16] S. Datta, *Quantum Transport: Atom to Transistor*. Cambridge, U.K.: Cambridge Univ. Press, 2005.

[17] S. Datta, "Nanoscale device modeling: The Green's function method," *Superlattice Microstruct.*, vol. 28, no. 4, pp. 253–278, Oct. 2000.

[18] (2011). *International Technology Roadmap for Semiconductors* [Online]. Available: http://www.itrs.net/Links/2011ITRS/Home2011.htm

Amretashis Sengupta (M'10) received the Ph.D. degree in engineering from Jadavpur University, Kolkata, India, in 2012.

He is currently a DST Post-Doctoral Fellow with the Department of Electronic Systems Engineering, Indian Institute of Science, Bangalore, India.

Ram Krishna Ghosh is currently pursing the Ph.D. degree with the Nano Scale Device Research Laboratory, Department of Electronic Systems Engineering, Indian Institute of Science, Bangalore, India.

Santanu Mahapatra (M'08–SM'10) received the Ph.D. degree from the Ecole Polytechnique Federale de Lausanne, Lausanne, Switzerland, in 2005.

He is currently an Associate Professor with the Indian Institute of Science, Bangalore, India.